J Solid State Electrochem (2006) 10: 283–287
DOI 10.1007/s10008-005-0695-1

ORIGINAL PAPER

Lihong Yu · Yuliang Cao · Hanxi Yang · Xinping Ai

Synthesis and electrochemical properties of high-voltage $LiNi_{0.5}Mn_{1.5}O_4$ electrode material for Li-ion batteries by the polymer-pyrolysis method

Received: 1 December 2004 / Accepted: 12 April 2005 / Published online: 8 June 2005

Abstract A submicron $LiNi_{0.5}Mn_{1.5}O_4$ cathode was synthesized via the pyrolysis of polyacrylate salts as precursor polymerized by reaction of the metal salts with acrylate acid. The structure and morphology of the resulting compound was characterized by powder X-ray diffraction (XRD) and transmission electron microscopy (TEM). The results reveal that the prepared $LiNi_{0.5}Mn_{1.5}O_4$ cathode material has a pure cubic spinel structure ($Fd\bar{3}m$) and submicron-sized morphology even if calcined at 900 °C and quenched to room temperature. The $LiNi_{0.5}Mn_{1.5}O_4$ electrodes exhibited promising high-rate characteristics and delivered stable discharge capacity (90 mAh/g) with excellent retention capacity at the current density of 50 mA/g between 3.5 and 4.9 V. The capacity of the $LiNi_{0.5}Mn_{1.5}O_4$ electrodes remains stable even after 30 cycles at low or high current density. This polymer-pyrolysis method is simple and particularly suitable for preparation of the spinel $LiNi_{0.5}Mn_{1.5}O_4$ cathode material compared to the conventional synthesis techniques.

Keywords Polymer-pyrolysis · High-voltage electrode · Lithium-ion battery

Introduction

Spinel $LiMn_2O_4$ is one of the potential candidates for the cathode materials for secondary lithium-ion battery due to its low cost and non-toxicity compared with currently used $LiCoO_2$. It is well known that the spinel $LiMn_2O_4$ material shows good stability during cycling and presents a 120 mAh/g capacity between 3.5 and 4.3 V. In order to improve performance of advanced rechargeable lithium-ion batteries including high output voltage, a number of research groups have reported transition metal-substituted spinel $LiM_xMn_{2-x}O_4$ materials (M = Cr, Co, Fe, Ni, Cu, etc.) due to the high-voltage plateau at around 5 V [1–11]. Among these materials, $LiNi_{0.5}Mn_{1.5}O_4$ has received much attention because of its high capacity and stable cycleability.

In general, spinel $LiNi_{0.5}Mn_{1.5}O_4$ can be prepared by solid-state reaction [1, 12] and sol–gel methods [13–15]. However, the solid-state reaction method has many disadvantages such as nonhomogeneity, control of stoichiometry that is not easy, longer calcinating time and large particle size with a broad distribution. Another approach, 'sol–gel' method, can produce better crystal homogeneity and electrochemical performances, but this synthetic procedure also has some disadvantages such as very time-consuming and complicated synthetic routes and high synthetic cost. Therefore, it is of practical importance to seek a simplified synthetic process for preparing the spinel $LiNi_{0.5}Mn_{1.5}O_4$ material.

In this paper, we report a polymer-pyrolysis route to synthesize $LiNi_{0.5}Mn_{1.5}O_4$ powder. The main advantage of this method is that the synthetic process is simple and easy to control [16]. In addition, it is advantageous to gain the pure submicron compound with uniformly distributed size. We also describe the structural and electrochemical properties of these compounds as intercalating cathode materials.

Experimental

Submicron $LiNi_{0.5}Mn_{1.5}O_4$ cathode material was prepared by a polymer-pyrolysis method using polyacrylates of Li, Ni and Mn as precursor compounds [16]. The copolymeric precursor was made from the solution polymerization of LiOH, $Ni(NO_3)_2$, $Mn(NO_3)_2$ and acrylic acid using $(NH_4)_2S_2O_8$ as initiator. The typical experimental procedure is first to dissolve a stoichiometric amount of LiOH, $Ni(NO_3)_2$ and $Mn(NO_3)_2$ in

L. Yu · Y. Cao (✉) · H. Yang · X. Ai
Department of Chemistry,
Wuhan University,
China, 430072
E-mail: ece@whu.edu.cn
Tel.: +86-27-68754526
Fax: +86-27-87884476

acrylic acid and to polymerize the precursor solution to form polyacrylates of Li, Ni and Mn at 80 °C. The resulting polyacrylates were dried at 120 °C for 24 h. The copolymeric precursor obtained was then decomposed at 450 °C for 5 h in air to obtain the Li–Ni–Mn oxide powders. In order to obtain homogeneous crystalline structure of the compounds, the precursor powders were finally calcined at 900 °C for 3 h in air and then quenched to room temperature. In order to demonstrate the effects of quenching and annealing on terminal materials, the precursor powders were calcined at 900 °C for 3 h in air and then cooled slowly in the oven. The actual stoichiometric composition of the thus prepared cathode was determined by inductively coupled plasma (ICP) analysis. The oxidation state of manganese cations was assessed by titration using $KMnO_4$ and $FeSO_4$. The cathode was dissolved in a large quantity of $FeSO_4$ aqueous solution containing H_2SO_4. The excess $FeSO_4$ was titrated using $KMnO_4$ solution. Subsequently, $Na_4P_2O_7{\cdot}10H_2O$ was added to adjust pH to 6–7. Based on the conservation of mass and charge, the average valence of manganese can be calculated.

The cathode electrode was prepared by mixing the $LiNi_{0.5}Mn_{1.5}O_4$ cathode material, acetylene black and polytetrafluoroethylene (PTFE) emulsion with isopropanol to form an electrode paste, then rolling the paste into a ca. 0.1 mm thick film and finally pressing the electrode film onto the aluminum foil of 2 cm^2 . The cathode electrode film consisted of 80% $LiNi_{0.5}Mn_{1.5}O_4$ powder, 12% acetylene black and 8% PTFE by weight.

The charge–discharge measurements were performed using a three-electrode test cell of a sandwich design. The $LiNi_{0.5}Mn_{1.5}O_4$ electrode and lithium electrode were separated by a microporous membrane (Celgard 2400) and pressed together parallelly by a pair of electrode holders. A small piece of lithium foil immersed in the electrolyte served as a reference electrode. The electrolyte was 1 mol L^{-1} $LiPF_6$ dissolved in a mixed solution of ethylene carbonate (EC)/dimethyl carbonate (DMC)/ethyl-methyl carbonate (EMC) (1:1:1). All the cells were assembled in a dry box filled with argon gas (Ar% > 99.99%, H_2O < 15 ppm, O_2 < 10 ppm). The galvanostatic charge–discharge test was conducted by a BTS-55 Neware Battery Testing System. We used different cells for each current density test. The cyclic voltammetry was carried out with CHI600A Eletrochemical Workstation.

In order to reveal the crystal structure of the $LiNi_{0.5}Mn_{1.5}O_4$ powders, X-ray diffraction (XRD) was employed using a Shimadzu XRD-6000 diffractometer with Cu K_α radiation. Transmission electron microscopy (TEM) was carried out with JEM-2010 system.

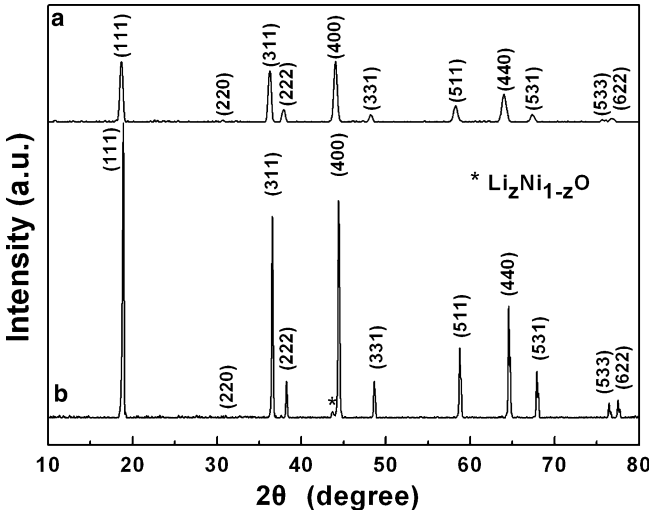

Fig. 1 XRD patterns of the $LiNi_{0.5}Mn_{1.5}O_4$ materials calcined at 900 °C in air for 3 h with (**a**) quenching; (**b**) annealing

Results and discussion

Structural characterization

Figure 1a shows the XRD profile of $LiNi_{0.5}Mn_{1.5}O_4$ quenched after being calcined at 900 °C for 3 h in air. As shown in Fig. 1a, the positions and diffraction intensities of the XRD peaks can be indexed by comparison to those of $LiMn_2O_4$ [13, 17–19], indicating that the material has a cubic spinel structure (space group: $Fd\bar{3}m$). The $LiNi_{0.5}Mn_{1.5}O_4$ material quenched from 900 °C shows a phase-pure cubic spinel structure without any impurities of NiO, which is indicated by the XRD peaks of $2\theta = 37.5°$, 43.8° and 63.8° in XRD patterns. In comparison with earlier reference [2], the $LiNi_{0.5}Mn_{1.5}O_4$ material quenched from high temperature was very difficult to obtain in a phase-pure cubic spinel structure without residual NiO impurities due to the oxygen loss at high temperature. Dahn and co-workers [2] reported that the formation of the NiO impurity resulted from the removal of a small amount of Ni from the $LiNi_{0.5}Mn_{1.5}O_4$ structure, which was due to excessively rapid cooling and insufficient oxygen uptake during cooling of the sample. Sun and co-workers [17] reported that the formation of the NiO impurity resulted from a small amount of residual nickel component in the $LiNi_{0.5}Mn_{1.5}O_4$ structure, which was due to some manganese loss during the formation of Li_2MnO_3 at 900 °C. However, the $LiNi_{0.5}Mn_{1.5}O_4$ material quenched from 900 °C was obtained by polymer-pyrolysis method without any NiO impurities. A possible explanation is that a small fraction of Ni that occupies tetrahedral position, 8a, is not removed from the spinel structure during rapid cooling due to submicron size and homogeneous distribution of the metallic ions in the structure of the $LiNi_{0.5}Mn_{1.5}O_4$ material prepared by the polymer-pyrolysis method.

In order to compare quenching process with annealing process, the diffraction pattern of the $LiNi_{0.5}Mn_{1.5}O_4$ material cooled slowly is obtained as shown in Fig. 1b. The diffraction patterns in Figs.1a and 1b show some clear difference. First, peaks of the NiO impurity phase are clearly visible (indicated by asterisk) in Fig.1b. This

is because a few Ni cations are not removed from the tetrahedral position (8a) back to octahedral position (16d), but from the spinel structure to form NiO impurity due to oxygen uptake during slow cooling. Second, in comparison with the diffraction pattern of the slowly cooled material shown in Fig. 1b, the intensity of (220) reflection increased and the I_{111}/I_{311} ratio decreased in the diffraction pattern of the quenched material shown in Fig. 1a. This result confirms that the tetrahedral position was occupied by the transition element, Ni [20]. Third, the lattice parameters of the $LiNi_{0.5}Mn_{1.5}O_4$ cathode materials with annealing or quenching calculated from the XRD patterns based on the cubic structure model are 8.1545 Å or 8.2263 Å, respectively. These results are consistent with those reported by Dahn et al. [2]. The increase of the lattice constant of the spinel phase is due to the excess Mn^{3+} in lattice structure, which resulted from the oxygen deficiency in quenched samples. The oxygen deficiency of the quenched sample can be deduced from the precise molecular formula $Li_{0.93}Ni_{0.501}Mn_{1.50}O_{3.74}$ calculated on the basis of the ICP results. It indicates that there is a large amount of oxygen deficiency and low-average-oxidation-state (3.70) Mn cations in lattice structure. The Mn average oxidation state of the samples in annealing or quenching, which was determined by the redox titration, is 3.98 or 3.65, respectively. This result is consistent with that calculated from the molecular formula. It demonstrates that the quenching process accelerates the formation of Mn^{3+} in the terminal product due to oxygen loss in the sample, in agreement with those obtained from the diffraction patterns.

Figure 2 shows the TEM image of the prepared $LiNi_{0.5}Mn_{1.5}O_4$ material calcined at 900 °C and quenched to room temperature. It can be clearly seen from Fig. 2 that the $LiNi_{0.5}Mn_{1.5}O_4$ material is composed of ultrafine particles with uniformly distributed size of ca. 200 nm with octahedral shape. The results demonstrate that the Li–Ni–Mn–O compounds made by the polymer-pyrolysis method have a cubic spinel structure. Figure 2 also demonstrates that the material exhibits well-dispersed particles. It is inferred that such submicron particles would facilitate reducing the diffusion length of the lithium ions during the course of intercalation and deintercalation, and therefore lead to excellent high-rate dischargeability of the $LiNi_{0.5}Mn_{1.5}O_4$ cathode by the polymer-pyrolysis method.

Electrochemical behaviors

Figure 3 gives a typical cyclic voltammogram of a $LiNi_{0.5}Mn_{1.5}O_4$ electrode in 1 M $LiPF_6$ + EC/DMC/EMC solution. The voltammogram shows three oxidation peaks appearing at 4.15, 4.72 and 4.88 V respectively, but only two reduction peaks are observable at 4.6 and 3.9 V on the reverse scan. This CV features are virtually analogous to those of $LiNi_{0.5}Mn_{1.5}O_4$ cathode as Aurbach et al. [21] reported. According to their previous assignments of the CV features, the tiny anodic and cathodic peaks around 4 V are due to the redox reaction of Mn^{3+}/Mn^{4+} couple, and the remarkable redox peaks around 5 V are related to the Ni^{2+}/Ni^{3+} and the Ni^{3+}/Ni^{4+} couples. These assignments of the CV peaks can also be applicable for the CV features of the $LiNi_{0.5}Mn_{1.5}O_4$ cathode prepared by polymer-pyrolysis method as shown in Fig. 3. Compared with the CV features observed for the samples prepared by solid-state method [3] or sol–gel method [14], the pair of CV peaks at 4.0 V appears more prominent for the $LiNi_{0.5}Mn_{1.5}O_4$ prepared by polymer-pyrolysis method. As suggested by Dahn [2], Mn^{3+} in the $LiNi_{0.5}Mn_{1.5}O_4$ structure is formed to meet the charge balance of the composition due to ejection of oxygen during calcination. The observation of stronger CV peaks at 4.0 V for the pyrolyzed $LiNi_{0.5}Mn_{1.5}O_4$ may imply a larger oxygen

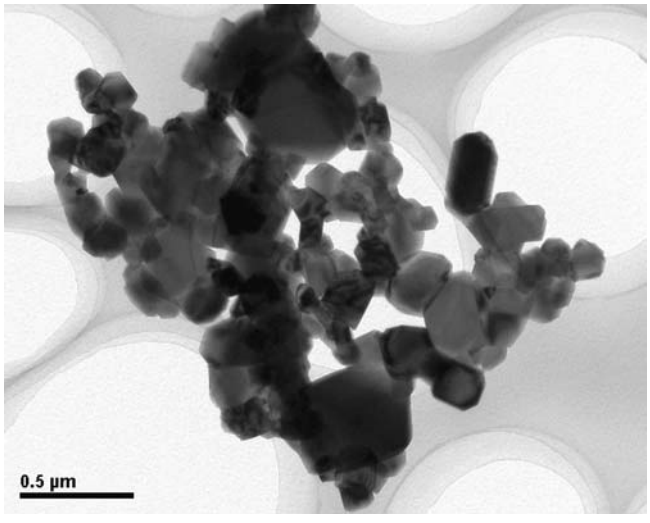

Fig. 2 A TEM micrograph of $LiNi_{0.5}Mn_{1.5}O_4$ material calcined at 900 °C in air for 3 h with quenching

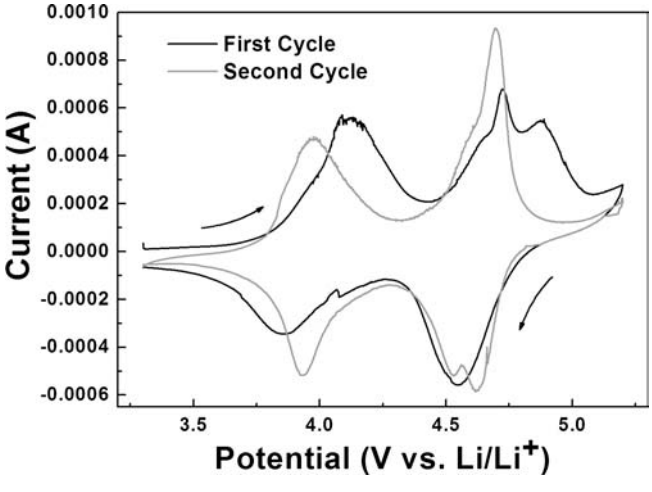

Fig. 3 Cyclic voltammograms of quenched $LiNi_{0.5}Mn_{1.5}O_4$ electrode in 1 M $LiPF_6$ + EC/DMC/EMC (1:1:1) solution. Scan rate: 0.1 mV/s

loss of the $LiNi_{0.5}Mn_{1.5}O_4$ powder during polymer-pyrolysis and following the calcination process at 900 °C. This result is coincident with that of the chemical analysis. In addition, it can be seen that the voltage intervals between the corresponding cathode peak and anode peak decreases with the cycling. It indicates that the lithium intercalation/deintercalation process becomes more reversible with cycling.

Figure 4 shows the charge–discharge profiles of the $LiNi_{0.5}Mn_{1.5}O_4$ material quenched from 900 °C and cycled between 3.5 and 4.9 V at a current density of 50 mA/g. In agreement with the CV features, the first charging curve of $LiNi_{0.5}Mn_{1.5}O_4$ electrode shows three voltage plateaus at 4.1, 4.7 and 4.8 V, respectively, and the first discharge profile gives two voltage plateaus at 4.6 and 3.95 V, respectively. As mentioned above, the charging and discharging reactions at the voltage around 4.0 V are due to the red-ox reactions of Mn^{3+}/Mn^{4+} couple and the voltage plateaus at around 4.7 and 4.8 V during the first charge process correspond to the oxidation reaction of Ni^{2+}/Ni^{3+} and Ni^{3+}/Ni^{4+} couples, respectively. However, during the successive charge–discharge processes, the two charge plateaus at around 4.7 and 4.8 V become indistinguishable compared with the first charge curve. This indicates that the lithium intercalation/deintercalation process becomes more reversible with cycling, which is consistent with what was discussed for the voltammogram curves, as shown in Fig. 3. In the first charge–discharge process, the discharge capacity is about 90 mAh/g with the irreversible capacity of 33% and the discharge curves show two potential plateaus at around 4.0 and 4.7 V, corresponding to the rechargeable capacity of 45 mAh/g and 45 mAh/g, respectively. From the second cycle, the coulombic efficiency of the electrode increases rapidly to 90%.

It is well known that the theoretical capacity of the $LiNi_{0.5}Mn_{1.5}O_4$ cathode is estimated at 147 mAh/g, corresponding to the removal of the whole lithium from the cathode. In previous reports [13], the discharge capacity of the $LiNi_{0.5}Mn_{1.5}O_4$ cathode is usually observed to be 130 mAh/g, about 90% of the theoretical capacity. However, the $LiNi_{0.5}Mn_{1.5}O_4$ cathode in the present study only gives less discharge capacity of about 90 mAh/g probably because it is difficult for Ni^{2+} in the tetrahedral positions to be oxidized to Ni^{4+} .

Figure 5 shows the capacity retention versus cycle number for the $Li/LiNi_{0.5}Mn_{1.5}O_4$ cells cycled at the voltage interval of 3.5–4.9 V during the first 30 cycles at various rates. In this test, the quenched $LiNi_{0.5}Mn_{1.5}O_4$ material was used. The initial discharge capacity was about 90 mAh/g at a specific current of 50 mA/g and the discharge capacity observed at a specific current of 200 mA/g was still about 70 mAh/g. However, at a specific current of 400 mA/g, the initial discharge capacity of the $LiNi_{0.5}Mn_{1.5}O_4$ electrode decreased to about 40 mAh/g, probably due to the slow diffusion rate in solid-state structure. From the cycling performance it can be seen that the prepared material cycled at both low specific current and high specific current has good retention capacity. These results clearly demonstrate that the $LiNi_{0.5}Mn_{1.5}O_4$ electrode delivers a high-rate characteristic and quite a stable cycling capacity when cycled between 3.5 and 4.9 V, even at the presence of some quantity of Mn^{3+} in the $LiNi_{0.5}Mn_{1.5}O_4$ material. It can be seen that the discharge capacity of the $LiNi_{0.5}Mn_{1.5}O_4$ electrode at over 50 mA/g decreased first, then increased to a stable value with cycling. In the initial cycling process, the decrease of discharge capacity is because the Ni cations in tetrahedral positions hinder the movement of the lithium ion. Particularly, this phenomenon becomes more remarkable at the high

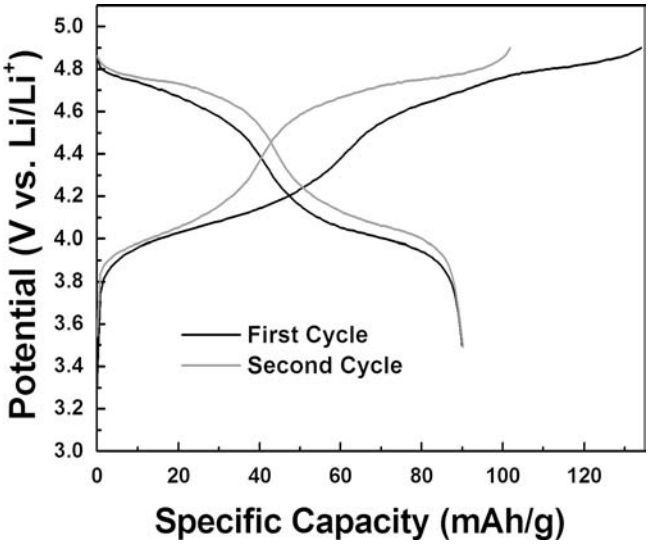

Fig. 4 The first two charge–discharge curves for Li/(quenched) $LiNi_{0.5}Mn_{1.5}O_4$ cells cycled at a current density of 50 mA/g at 3.5–4.9 V

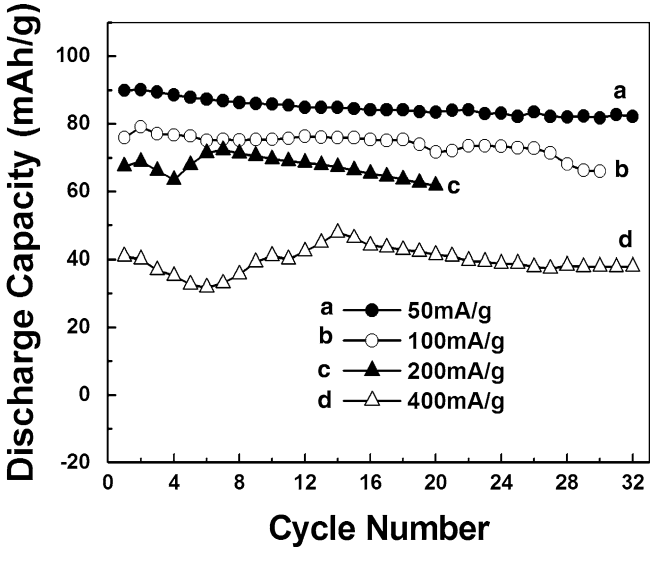

Fig. 5 Capacity retention versus cycle number for Li/(quenched) $LiNi_{0.5}Mn_{1.5}O_4$ cells cycled between 3.5 and 4.9 V at a current density of (**a**) 50 mA/g; (**b**) 100 mA/g; (**c**) 200 mA/g; (**d**) 400 mA/g

charge/discharge specific current (400 mA/g). However, the lithium intercalation/deintercalation reaction becomes more reversible with cycling. Thus the discharge capacity gradually increases up to a stable value. In a previous work [2], it is very difficult for the $LiNi_{0.5}Mn_{1.5}O_4$ material quenched from high temperature to obtain the high capacity and stable cycling performance due to the removal of Ni from the spinel structure and the dissolution of Mn resulting from the disproportionate Mn^{3+} in lattice structure. However, the quenched $LiNi_{0.5}Mn_{1.5}O_4$ material prepared by the polymer-pyrolysis method demonstrates the stable cycling performance. A reasonable explanation is that the Ni deficiency in the spinel structure did not occur during quenching due to the homogeneous distribution and submicron granularity of the sample by the polymer-pyrolysis method. Thus the integrity of the lattice is retained improving the cycling performance of the $LiNi_{0.5}Mn_{1.5}O_4$ material.

Conclusion

This paper describes a novel route of producing homogeneous submicron $LiNi_{0.5}Mn_{1.5}O_4$ materials by the polymer-pyrolysis method using a Li–Ni–Mn copolymeric precursor polymerized from the acrylates solution. The data from the XRD and TEM measurements revealed that the $LiNi_{0.5}Mn_{1.5}O_4$ material quenched from 900 °C has good crystallinity with a pure cubic spinel structure and a uniformly distributed size of ca. 200 nm. The charge–discharge experiments demonstrate that the quenched $LiNi_{0.5}Mn_{1.5}O_4$ electrode has a specific discharge capacity of 90 mAh/g and a good cycling stability during the cycling voltage interval of 3.5–4.9 V. In addition, the prepared $LiNi_{0.5}Mn_{1.5}O_4$ electrode exhibits an excellent cycling stability even at high current density. Since the polymer-pyrolysis method is simple and it is easy to control the structure and morphology of the reaction product, it could be used for industrially producing highly homogeneous Li–Ni–Mn–O compounds.

Acknowledgements The authors sincerely acknowledge the financial support by the 973 Program, China (Grant No. 2002CB211800) and the technical assistance in TEM work by the Center for Electron Microscopy, Wuhan University.

References

1. Amine K, Tukamoto H, Yasuda H, Fujita Y (1996) J Electrochem Soc 143:1607
2. Zhong Q, Bonakdarpour A, Zhang M, Gao Y, Dahn JR (1997) J Electrochem Soc 144:205
3. Ohzuku T, Takeda S, Iwanaga M (1999) J Power Sources 81:90
4. Lee YS, Todorov YM, Konishi T, Yoshio M (2001) ITE Lett 1:1
5. Sigala C, Guyomard D, Verbaere A, Piffard Y, Toumoux M (1995) Solid State Ionics 81:167
6. Gao Y, Myrtle K, Zhang M, Reimers JN, Dahn JR (1996) Phys Rev B 54:16670
7. Ohzuku T, Ariyoshi K, Takeda S, Sakai Y (2001) Electrochim Acta 46:2327
8. Ein-Eli Y, Vaughey JT, Thackeray MM, Mukerjee S, Yang XQ, McBreen J (1999) J Electrochem Soc 146:908
9. Kawai H, Nagata M, Tukamoto H, West AR (1999) J Power Sources 81–82:67
10. Shigemura H, Sakaebe H, Kageyama H, Kobayashi H, West AR, Kanno R, Morimoto S, Nasu S, Tabuchi M (2001) J Electrochem Soc 148:A730
11. West AR, Kawai H, Kageyama H, Tabuchi M, Nagata M, Tukamoto H (2001) J Mater Chem 11:1662
12. Guohua L, Ikuta H, Uchida T, Wakihara M (1996) J Electrochem Soc 143:178
13. Sun YK, Lee YS, Yoshio M, Amine K (2002) Electrochem Solid-State Lett 5:A99
14. Alcantara R, Jaraba M, Lavela P, Tirado JL (2002) Electrochem Acta 47:1829
15. Amine K, Tukamoto H, Yasuda H, Fujita Y (1997) J Power Sources 68:604
16. Yu LH, Yang HX, Ai XP, Cao YL (2005) J Phys Chem B 109:1148
17. Kim JH, Myung ST, Sun YK (2004) Electrochim Acta 49:219
18. Lee YS, Sun YK, Ota S, Miyashita T, Yoshio M (2002) Electrochem Commun 4:989
19. Ohzuku T, Kitagawa M, Hirai T (1990) J Electrochem Soc 137:769
20. Caballero A, Cruz M, Hernan L, Melero M, Morales J, Castellon ER (2005) J Electrochem Soc 152 (3):A552
21. Markovsky B, Talyossef Y, Salitra G, Aurbach D, Kim HJ, Choi S (2004) Electrochem Commun 6:821